PROCEEDINGS OF SCIENCE

The High Time Resolution Spectrometer (HTRS) aboard the International X-ray Observatory (IXO)

Didier Barret*, **Laurent Ravera, Carine Amoros, Martin Boutelier, Jean-Michel Glorian, Olivier Godet, Guillaume Orttner, Karine Lacombe, Roger Pons, Damien Rambaud, Pascale Ramon, Souad Ramchoun**
Institut de Recherche en Astrophysique et Planétologie
E-mail: didier.barret@cesr.fr

Pierre Bodin, Thierry Maciaszek, Jean-Marc Biffi, Marielle Belasic, Rodolphe Clédassou, Delphine Faye, Benjamin Pouilloux
Centre National d'Etudes Spatiales, 18 av Edouard Belin 31401 Toulouse Cedex, France

Christian Motch, Laurent Michel
Université de Strasbourg, Observatoire Astronomique, 11 rue de l'Université, 67000 Strasbourg France

Peter H. Lechner, Adrian Niculae
PNSensor GmbH, Otto-Hahn-Ring 6, 81739 München, Germany

Lothar W. Strueder
Max-Planck-Institut für extraterrestrische Physik Giessenbachstr., Garching, Germany

Giuseppe Distratis, Eckhard Kendziorra, Andréa Santangelo, Christoph Tenzer, Henning Wende
Institut für Astronomie und Astrophysik, Sand 1 D-72076 Tübingen, Germany

Joern Wilms, Ingo Kreykenbohm, Christian Schmid
Dr. Remeis-Observatory, Sternwartstr. 7, 96049 Bamberg, Germany

Stéphane Paltani, Franck Cadoux
ISDC, Geneva Observatory, Ch. d'Écogia 16, Ch-1290 Versoix, Switzerland

Carlo Fiorini, Luca Bombelli
Politecnico di Milano, Via Golgi 40, 20133 Milano Italy & INFN, Sezione di Milano, Via Celoria 16, 20133, Milano, Italy

Mariano Méndez
Kapteyn Astronomical Institute,P.O. Box 800, 9700 AV Groningen, The Netherlands

Sandro Mereghetti
INAF - Istituto di Astrofisica Spaziale e Fisica Cosmica - via Bassini 15, I-20133 Milano, Italy

PoS(HTRS 2011)003

PROCEEDINGS OF SCIENCE

The High Time Resolution Spectrometer (HTRS) is a non-imaging instrument, based on a monolithic array of Silicon Drift Detectors (SDDs) with 31 cells in a circular envelope and an X-ray sensitive volume of 4.5 cm^2 x 450 μm. It can perform observations of the brightest X-ray sources of the sky (up to 12 Crab) in the 0.3-15 keV range, with sub-millisecond time resolution, low deadtime, low pile-up (both much less than 2% at 1 Crab), and CCD type energy resolution (goal of 150 eV FWHM at 6 keV). In this paper, we present the mechanical, thermal and electrical design of the HTRS, as studied for the International X-ray Observatory [1]. We also illustrate its performance as assessed through Monte Carlo simulations.

Fast X-ray timing and spectroscopy at extreme count rates: Science with the HTRS on the International X-ray Observatory - HTRS2011,
February 7-11, 2011
Champery, Switzerland

*Speaker.

PoS(HTRS 2011)003

1. INTRODUCTION

Measuring the distribution of stellar mass black hole spins, constraining the equation of state of matter at supra-nuclear densities and probing strong field general relativity [2] require the capability to observe bright galactic X-ray binaries (black hole X-ray novae, type I X-ray bursters, ...), with count rates exceeding several hundred thousand counts per second up to a few millions (i.e. sources brighter than a few 100 mCrab up to several Crabs). The top level HTRS requirements, as derived for IXO, are listed in Table 1. In order to meet those requirements, the HTRS is made as an array of 31 silicon drift detectors (SDDs), operated out of focus, in such a way that the focal beam from the IXO mirrors is spread almost uniformly over the full array (the SDD array is described in details in a companion paper Lechner et al., same issue).

Table 1: The HTRS top level requirements

Max count rate (nominal)	2 Mcounts/s ($\sim$ 12 Crab)
Energy range	0.3-15 keV
Energy resolution @ 6 keV	$<$ 200 eV/150 eV (goal)
Minimum time resolution	10 microseconds
Deadtime @ 1 Crab	$<$ 2%
Pile-up @ 1 Crab	$<$ 2%

2. HTRS functional breakdown

The HTRS is made of two assemblies (see figure 1): The Focal Plane Assembly (FPA) including the Detector Unit (DU) and the filter wheel (FW) and the Electronics Box (EB) which includes the Pre-Processing Unit (PPU) and the Data Processing Unit (DPU).

In the Detector Unit (DU), the Front End Electronic (FEE) is located close to the detector array. It is made of 4 analog Application Specific Integrated Circuits (ASICs) that process the 31 detector signals. The FEE sends its outputs to the Pre-Processing Unit (PPU) which is located in the electronics box one meter away. The shaping of the detector signals and the detection of the events is partially done in the FEE and in the PPU. Two options (so-called analog shaping option and digital shaping option) are currently studied, with the baseline being the more advanced analog option. For each detected photon the PPU provides the raw data (amplitude and time) to the DPU.

We have designed the HTRS in order to reduce the impact of failures. The detector array, its associated readout electronics (FEE and PPU) and part of the power distribution are split in four quadrants. The DPU and part of the Power Conversion and Distribution Unit (PCDU) are used in cold redundancy. There are two DPUs and two PCDUs, but only one of each is on at any given time. The filter wheel uses a single motor equipped with two coils, so that it can be driven by both DPUs.

The preliminary CAD design of the HTRS FPA is shown in Fig. 2. The size, mass and power budgets of the HTRS are given in Table 2.

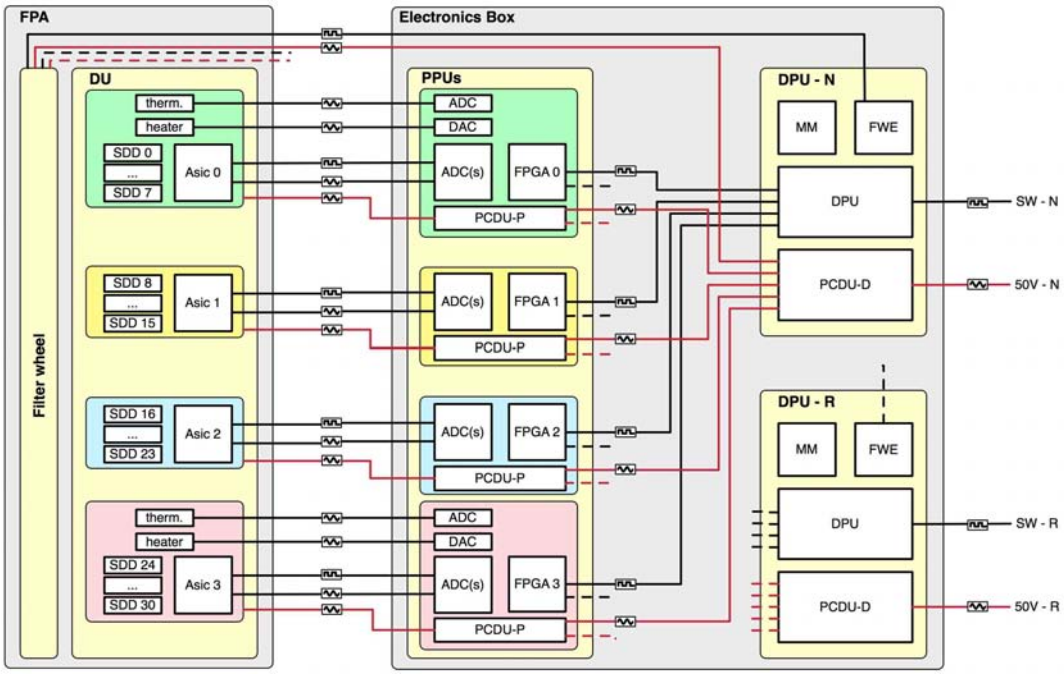

Figure 1: HTRS functional breakdown. The HTRS is made of two assemblies: the focal plane assembly (left) and the electronics box (right). The SDD readout electronics is located in the DU. The electronics box is located less than 1 meter away from the FPA. The DPUs are used in cold redundancy.

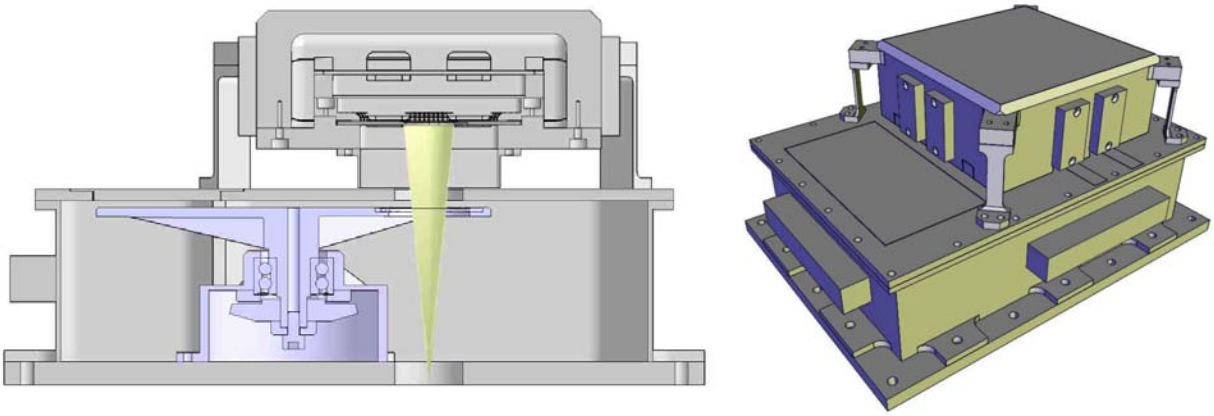

Figure 2: The CAD design of the HTRS FPA (cutaway view on the left and an external view on the right). The thermal decoupling between the FPA and DU is achieved through four titanium blades, located at each corner (see right hand side figure).

For the thermal architecture, we have considered that i) the temperature of the detector array should be -40±1°C during operations (the temperature is regulated by the HTRS DPU); ii) the cold interface with the spacecraft is regulated at -50±2.5°C in each HTRS mode (operating and non operating); iii) the Movable Instrument Platform (MIP) is at room temperature (the exact temperature range is not defined yet; it should be within -10°C and +40°C); and iv) the HTRS setting time (which includes the detector array thermal stabilization) should be as short as possible (shorter

Table 2: The HTRS size, mass and power budgets.

Dimensions	Mass with 20% contingency	Power at peak 70% DC-DC conv. eff.+ 20%margins
310x230x155 mm^3 (FPA) 360x233x175 mm^3 (electronics box)	30.3 kg	145 W

than 20 minutes). With all these constraints, we have chosen the thermal decoupling to be done between the FPA structure and the detector unit, using four titanium blades (see Fig. 2).

2.1 The Focal plane assembly

2.1.1 The detector unit (DU)

The HTRS instrument is based on a Silicon Drift Detector (SDD). The SDD principle uses a built-in potential gradient to collect radiation-generated electrons on a small sized anode (Fig. 3). That way the device combines a large sensitive area up to 1 cm^2 and a small value of the readout capacitance of the order of 100 fF [3]. The small capacitance allows X-ray spectroscopy measurements with CCD-like energy resolution ($\leq$ 150 eV FWHM at 6 keV) and high count rate capability up to 10^6 photons per second [4]. The integration of the first transistor of the amplifying electronics makes the sensor insensitive to microphonic noise and electronic pickup. The SDD concept is of enormous flexibility in the choice of sensor size and shape. By integrating a number of SDDs to a monolithic array, large sensitive areas can be obtained, while maintaining the performance properties of the single device [5].

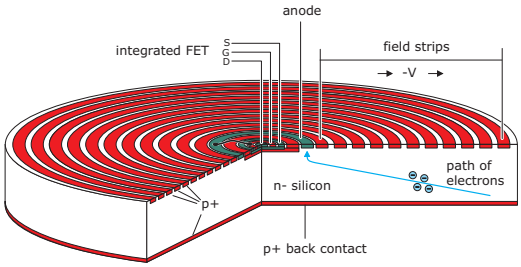

Figure 3: Schematic view of a cylindrical Silicon Drift Detector. Electrons are guided by a radial electric field generated by the system of concentric drift rings towards the small sized collecting anode and the readout transistor in the centre of the device.

The HTRS sensor is a multi-channel SDD consisting of 31 cells with a circular envelope of 24 mm diameter and a total area of 4.5 cm^2. The central cell is circular, the outer cells have the shape of ring sectors and are arranged in three rings of 1 x 6 and 2 x 12 cells (Fig. 4). All cells have equal areas of 14.6 mm^2 (to be exposed to comparable proton fluxes along the mission lifetime). The Silicon thickness is 450 μ [6].

One surface of the sensor is filled with the integrated readout structures and the drift ring system defining the collecting electric field. The 31 SDD cells are logically grouped in four quadrants

of seven or eight cells with redundant supply lines. Each quadrant is connected to an eight-channel readout ASIC. For each cell the sensor opposite surface includes a shallow non-structured junction acting as thin homogeneous entrance window for backside illumination. The boundaries between the cells entrance windows is masked by a ~ 200 μm wide baffle to exclude split events, i.e. photons depositing signal charges in neighboring cells, thus causing false energy information. A seven-cell prototype sensor with 7 x 10 mm^2 sensitive area, representative of the centre of the final HTRS device is currently in production.

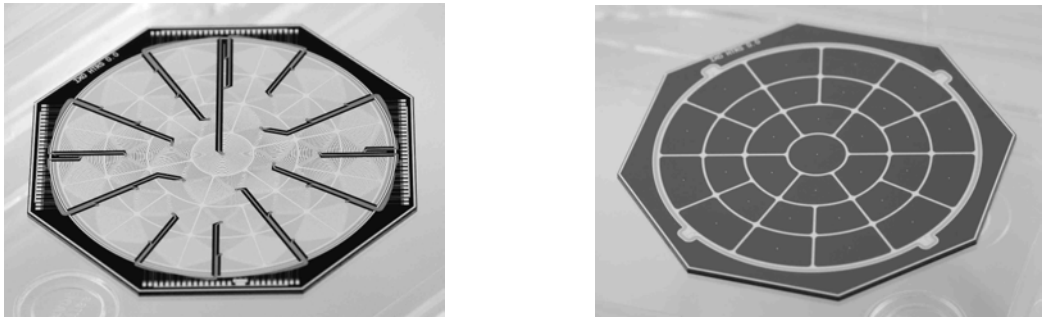

Figure 4: Mechanical sample of the HTRS sensor, readout side (left) and entrance window side (right). In the layout shown here the cell sizes vary with the radial position, the final design would have equal cell sizes.

At the HTRS experimental conditions, i.e. sensor temperature -40°C and short signal processing time for count rate handling, the SDD energy resolution should be ≤ 150 eV FWHM at 6 keV. The energy resolution is stable within 2% and the gain variation is less than 2 % even at count rates exceeding 10^5 photons per second and SDD cell, corresponding to a source intensity of ~ 20 Crab. SDDs processed in the technology relevant for the HTRS sensor have been proven to be radiation hard with respect to X-rays up to a number of 10^{13} absorbed photons. This figure would theoretically allow for a ten year continuous observation of bright sources with an intensity of several Crabs. In addition to photon irradiation, the HTRS sensor would have been exposed to 5×10^9 protons (10 MeV equivalent) per cm^2 during the mission lifetime (taken to be 10 years including a 5 year extension), assuming an effective shielding of 15 mm Al. Based on experimental data [7] the non-ionizing radiation effect has been modeled to cause a deterioration of the energy resolution, not exceeding 250 eV FHWM at 6 keV after 10 years of operation.

The thermal, mechanical and electrical interface to the HTRS sensor is given by the sensor hybrid. The hybrid contains passive RC-filter components, and per quadrant a power flex connection to the electronics box and a signal flex connection to the readout board. To keep the design as compact as possible, the active components of the readout electronics are placed on a separate readout board. A graded shield plate is inserted between the sensor hybrid and the readout board to minimize the X-ray fluorescence radiation seen by the sensor. Sensor hybrid and readout board are enclosed in an Al box acting both as radiation shield and thermal interface (Fig.5). The sensor assembly is mounted on a structure, with the sensor displaced from the focal plane by 11.3 cm in order to distribute the photon flux homogeneously over the 31 SDD cells.

2.1.2 The filter wheel

The filter wheel is a system to protect the detector, to reduce the optical loading on the SDD

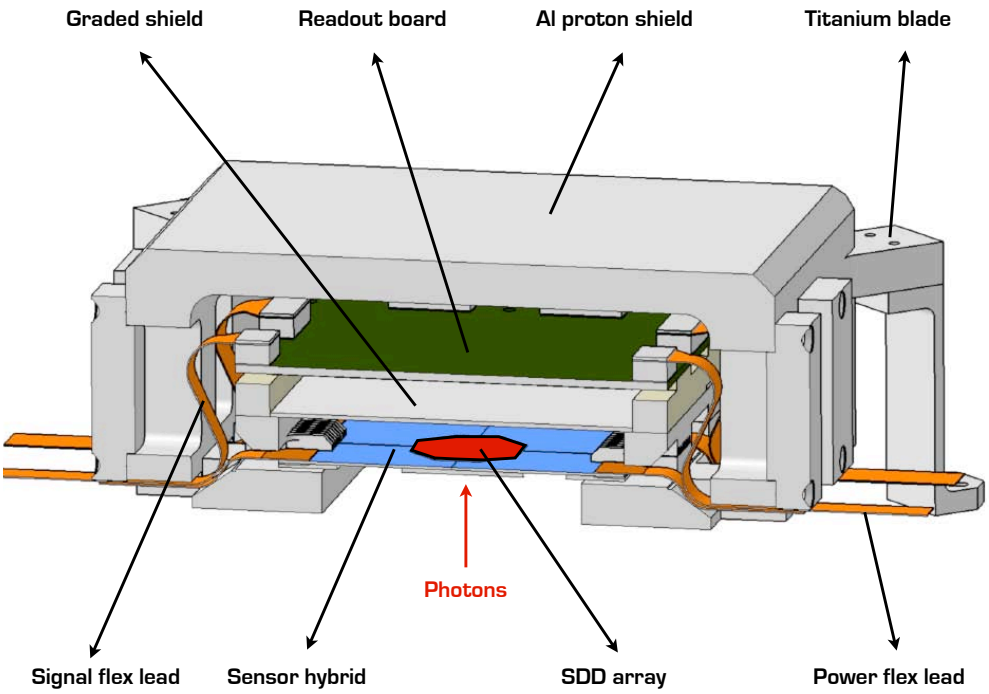

Figure 5: Cutaway view of the HTRS sensor assembly. The detector unit includes the detector hybrid, the readout FEE ASIC hybrid and flex interconnections. The SDD array is protected from radiations through a proton shield. The detector will be passively cooled and regulated at -40 °C.

array and to place a radioactive calibration source in the optical beam. It consists of a rotating disk perpendicular to the optical beam and is controlled by a motor. The motor is commanded by the DPU, which allows us to select accurately a specific orientation of the filter wheel. It is currently foreseen to have 5 positions:

1. Closed: The closed filter consists of a 50 μm Beryllium sheet. This provides protection against micro-meteorites of up to 7 μm diameter. The use of a moderately thick Beryllium filter, instead of a filter opaque in the X-rays, can also be a scientific advantage for the observation of extremely bright transients, since it cuts efficiently low-energy X-ray photons. It can also be used for instrument safety reasons protecting for instance against excessive charged particle flux (solar flare or local magnetospheric storms).

2. Open: In this position, the beam does not cross any material at the position of the filter wheel. This "filter" is the normal position for scientific operations.

3. Thin filter: This filter consists of a 30 nm layer of Aluminum deposited on a plastic support. The support is planned to be a 200 nm–thick film of polypropylene (C_nH_{2n}). The goal of this filter is to reduce the photon flux in the optical range by a factor about 100, while being as transparent as possible in the X-rays. This helps reducing the optical load of the detector, and therefore the noise and energy shift, when observing X-ray sources that are relatively bright in the optical.

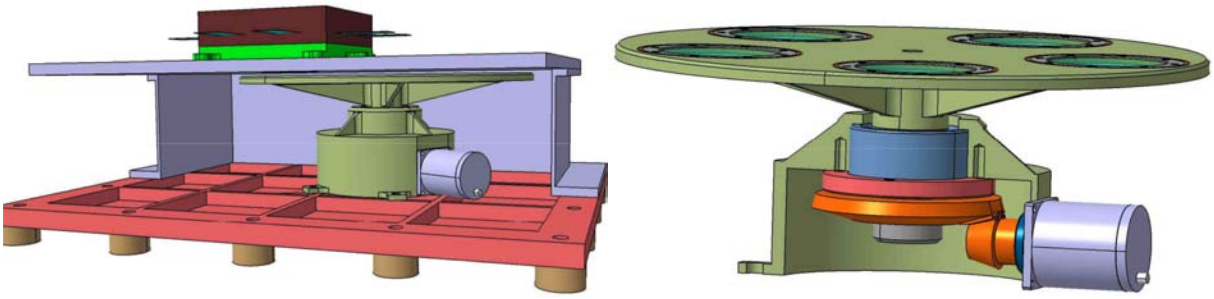

Figure 6: HTRS filter wheel. Left: Integrated view of the HTRS detector unit including its associated filter wheel. The filter wheel fits very closely into the FPA. Right: Cut-out view of the filter wheel with its 5 positions, showing the perpendicular mounting of the motor and the bevel gear.

4. Thick filter: This filter is identical to the thin filter, but the Aluminum layer is 50 nm thick. It is used in case of X-ray sources that are very bright in the optical.

5. Calibration sources: A filter containing a radioactive source can be put in and out of the beam in order to perform energy calibration measurements. The chosen radioactive element is ^{55}Fe, producing a Mn K$\alpha_{1,2}$ line around 5.9 keV. Its half-life of 2.73 yr is compatible with the relatively long foreseen lifetime of the IXO mission.

Fig. 6 shows the preliminary design of the filter wheel configuration. Except for the specific mechanism parts (motor, gears, bearings), which are mostly steel, and the filters, all elements of the filter wheel are in Aluminum. The total mass of the filter wheel is less than 800 g. The motor is a stepper motor with significant flight heritage. Redundancy is assured by the presence of double-winding. Because of the very limited height of the filter wheel, the motor has been placed horizontally, and the wheel axis is driven through a bevel gear. A planetary gear with moderate reduction could be fitted to the motor's axis if the torque of the motor proves insufficient. The axis is mounted on the wheel support using a single double-row pre-stressed ball bearing. The filter wheel is equipped with a system of control of the position, so that the central unit receives an independent acknowledgment that the correct filter position has been reached. This is realized by placing a redundant set of potentiometers on the tip of the axis.

The support structure of the wheel is machined out of a cylindrical block of Aluminum, providing an empty space in which all gears are located. Thanks to this design, any contaminant originating from the wearing of moving pieces or from the lubricant inside the gears or motor are trapped inside this cavity, and cannot reach the detector. A pipe (not shown on the figure) shall be fitted to the wheel support structure, so that the content of the cavity is evacuated outside of the HTRS. Contamination coming from the bearing is reduced by the presence of a labyrinth between the wheel and the support.

The wheel itself is composed of a disk mounted on a rotation axis. Ribs are added to the wheel to increase rigidity. The disk has five holes to allow the mounting of the different filters with 35 mm clear diameter. The thin, thick and closed (i.e., Beryllium) filters are all mounted on a similar annular mount, which is screwed directly onto the wheel.

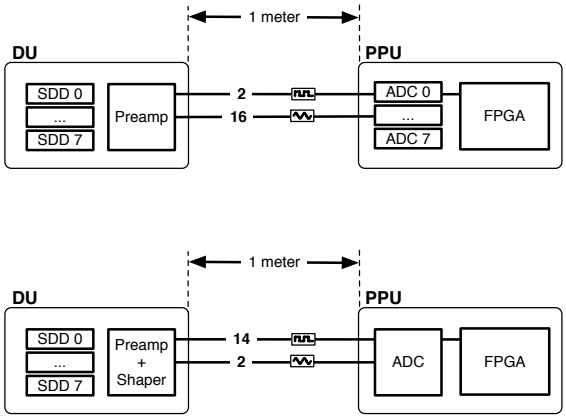

Figure 7: Two different implementations of the readout front-end electronics of the HTRS: the digital shaper option on top and the classical analog readout at the bottom.

Radioactive ^{55}Fe source is placed on one filter position. The radioactive sources are encapsulated in an Aluminum support which covers the back of the source. This acts as a collimator and shield, but also generates fluorescence Aluminum lines around 1.5 keV, which improves the determination of the energy calibration. With the requirement that pixels can be calibrated with better than 1% accuracy in a 1-minute exposure after 15 years, the source requires an activity at the time of launch of 3 MBq in total.

2.2 The HTRS electronics

2.2.1 Detector readout: analog and digital

To achieve an energy resolution and gain stability independent of the input count rate, the first integrated FET is configured as the input stage of the charge sensitive amplifier with capacitive feedback and pulsed reset[5]. Concerning the pulse processing electronics, two parallel developments are under study: a full analog chain (our current baseline) and a digital chain (Fig. 7). In the full analog option, each of the four FEE ASICs includes: 8 pre-amplifiers, 8 shaping amplifiers with a 600 ns peaking time, 8 peak stretchers and a 8 to 1 analogue multiplexer. In the PPU, the FEE output signals are digitized at moderate speed (10 MHz) to be de-multiplexed and to recover the event amplitudes. This option is currently studied by Politecnico de Milano.

In the digital option, each of the four FEE ASICs includes 8 pre-amplifiers only. In the PPU, the FEE output signals (one per SDD) are digitized at a high rate (40 to 100 MHz). Both the analog and digital solution use secondary shaper filters with a short peaking time of 200 ns in order to detects the events and identify pileup occurrences. This filter makes a non-optimal measurement of the event amplitude, while the slow filter with a peaking time of 600 ns is dedicated to the event amplitude measurement.

The main advantage of the full analog option is the simplicity of the PPU. There are only four Analogue to Digital Converters (ADCs) clocked at 10 MHz. Moreover the data processing is very simple. As a consequence the power consumption is lower in the analog option than in the digital one. On the other hand, the digital option offers a lot of versatility, with potentially improved performance (which can be further optimized in flight, see below).

2.2.2 The Data Processing Unit

The DPU is located in the science data flow between the PPUs and the spacecraft. Its main tasks are event-preprocessing, data compression and data formatting. Furthermore, it distributes and executes telecommands from the spacecraft, controls the heaters and the filter wheel and acts as an interface for the collection of housekeeping data. Fig. 8 shows a block diagram of the current baseline concept. The raw science data arrive in parallel for all 31 SDDs from the PPUs. An FPGA first adds a time tag and then applies a commandable linear gain correction for each pixel individually. Depending on the selected data format, the FPGA either collects an energy spectrum with selectable bin size and integration time or produces simple event packets. The standardized data products (see the section on data modes below) are always generated.

A CPU then collects the data from the FPGA and stores and compresses them in the internal HTRS mass memory. The DPU is in charge of transferring the compressed data to the spacecraft telemetry system. Different data compression levels and algorithms have been compared in order to reach high compression factors while keeping the output rate of the compressed telemetry packets compliant with the allocated telemetry rate. Those are being studied in more detail on a simulation platform for the currently foreseen Leon III CPU implementation.

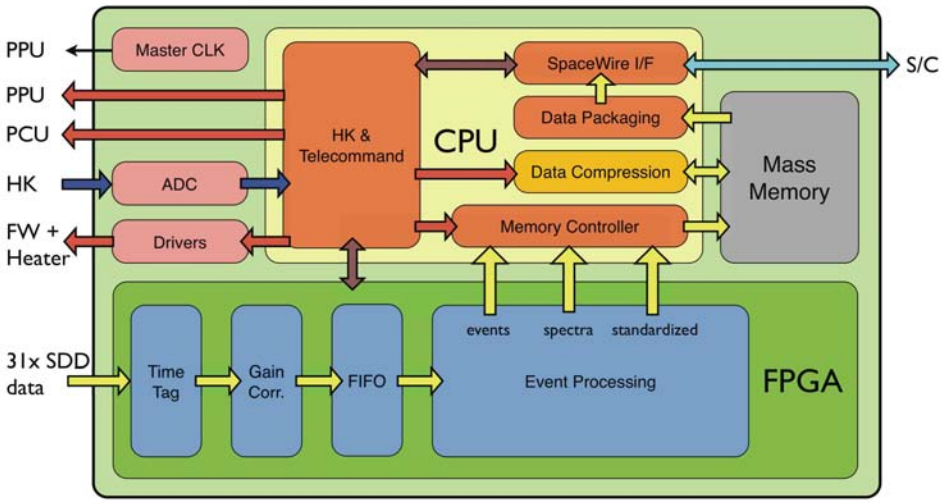

Figure 8: The Data Processing Unit block diagram with its main functionality identified.

3. Performance

3.1 The HTRS quantum efficiency

When computing the quantum efficiency of the HTRS, we have assumed that the entrance layer is made of a 30 nm of Al, which is the minimum that is technically feasible today. The thickness of the Al layer is still subject to optimization. It affects the quantum efficiency mostly in the low energy band, i.e. between 0.3 keV and 1.5 keV. Based on the XMM-pn CCD experience, we have also assumed a 6 nm Si dead layer, which represents the non depleted part of the diode entrance window. Transparencies of the filters have been estimated through Monte Carlo simulations. Cross

sections were provided by the EPICSHOW software v 98-1, which uses the EPIC (Electron Photon Interaction Code) data libraries. In addition, as mentioned above, a mask is required to avoid split events. In our baseline, we have assumed a mask with 200 μm spoke width.

For the nominal case (i.e. perfect alignment), an out-of-focus distance of 11.3 cm and a 24 mm diameter array, the mask represents a covered area fraction of 10%. The mask is opaque to X-rays up to 20 keV. The covered fraction of the mask is determined by the overall size of the detector, the number and size of the SDD cells. There is a trade-off between the count rate performance of the HTRS and the number of cells, over which the focal beam is spread. There is also a trade-off between the size of the SDD cell and the energy resolution degradation (leakage current increase) in response to proton irradiation (the bigger the cell, the faster the degradation at a given operating temperature). An optimization study through simulations to further reduce the mask loss fraction is on going. First results still indicate that a 10% estimate for the loss due to the mask is rather on the high side.

Based on the assumptions mentioned above, the quantum efficiency of the HTRS is shown in Fig. 9 for the open, thin and thick filter positions. As can be seen, the QE of the HTRS between $\sim$ 2 and 10 keV is determined by the fraction of photons absorbed in the mask used to avoid split events in the detector. At energies below 1.5 keV the quantum efficiency is set by the thin layer of Aluminum placed on the SDD bulk. Baseline optical filters (which are also subject to optimization) further attenuate the energy response below $\sim$ 3 keV.

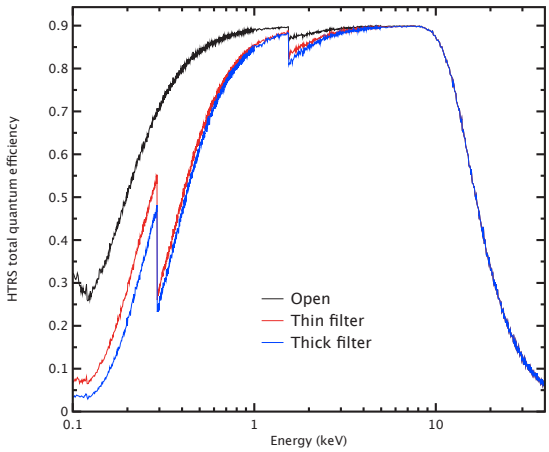

Figure 9: Quantum efficiency of the HTRS array with the mask (assuming an absorption of 10%) and the three filter positions.

3.2 The HTRS effective area

Along the ESA industrial studies, the effective area curves of the HTRS have been generated with the current IXO mirror response and the quantum efficiency curves presented in Fig. 9 (courtesy of Tim Oosterbroek). The effective area of the HTRS compared with the XMM-Newton EPIC-PN one is shown in Fig. 10. Note that compared with XMM-Newton (thin filter), the effective area at 6.4 keV is increased by a factor of about 17. To illustrate what such increase in effective area means, we have simulated a 1 second Crab observation by the HTRS. The observed unfolded

spectrum is shown in Fig. 10. The Crab currently produces about 170 000 counts/s over the whole energy range.

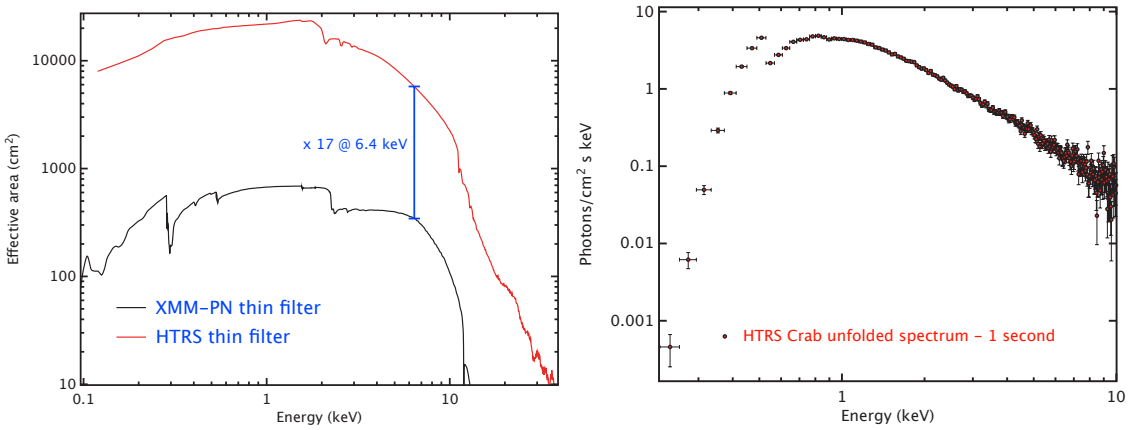

Figure 10: Left) HTRS effective area, compared with the XMM-Newton EPIC-PN one: there is a factor of 17 between the effective area at 6.4 keV between the two instruments. Right) HTRS unfolded Crab spectrum as observed during a 1 second exposure.

3.3 Detection efficiency: analog versus digital readout

The performance of the HTRS with respect to pile-up for observations of bright X-ray sources has been determined by simulations and analytical estimates [8]. The Monte-Carlo simulations are based on individual photons generated by a time-varying Poisson process generator [9] with realistic energy spectra and optional red-noise behavior [10].

The photons are distributed among the HTRS SDD pixels using a PSF for the particular out-of-focus position as shown in Fig. 11, which has been calculated for the Silicon Pore Optics mirror design according to mirror data provided by Tim Oosterbroek. Apart from the nominal alignment case we have also taken into account possible alignment margins in order to investigate the performance of the HTRS for these scenarios.

In both the analog and digital shaper options, there exists a minimum time (T_2) below which two photons are counted as one, with the energy of the resulting event being the sum of the energy of the two photons. This is what defines pile-up (those events are not good for science). For the analog option, the minimum time is 200 ns. It is comparable for the digital solution if the ADC rate is 40 MHz, but decreases to 80 ns if the ADC speed is 100 MHz. On the other hand, clean events, i.e. events for which both the time and energy can be reconstructed accurately must be separated in time by $T_1 = 1100$ ns (analog option) and $T_1 = 1250$ ns (digital option with an ADC rate of 40 MHz) or $T_1 = 500$ ns (digital option with an ADC rate of 100 MHz). For two photons falling in a time interval comprised between T_2 and T_1, in the analog option, two photons are counted. However, only the energy of the first event is measured with reduced accuracy (using the output of the fast 200n s shaper), while the second event is discarded due to limitation in the multiplexing speed. On the other hand, in the digital option, two photons are counted and their energy is measured with a reduced accuracy (those events are good for science). The pile-up and good event fractions are

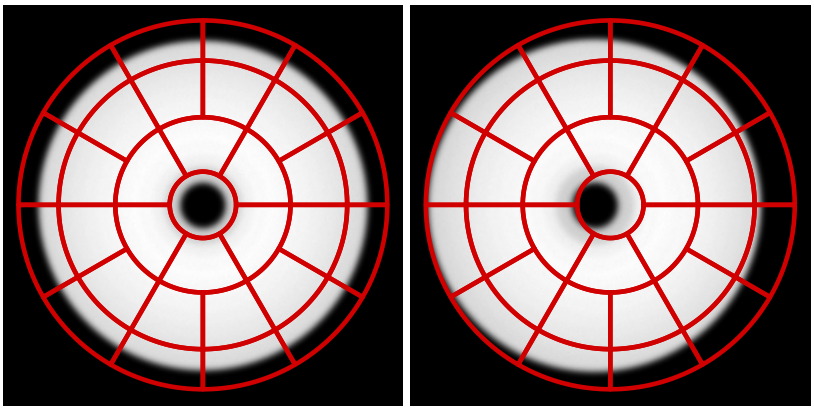

Figure 11: Distribution of 1 keV photons on the HTRS detector at an out-of-focus distance of 11.3 cm, according to mirror data provided by Tim Oosterbroek. The left-hand image displays the PSF for the nominal alignment, whereas in the right-hand image the PSF is shifted with respect to the central position assuming a combination of all possible alignment inaccuracies. In this worst case scenario still 99.9% of the incident photons are located within the detector radius.

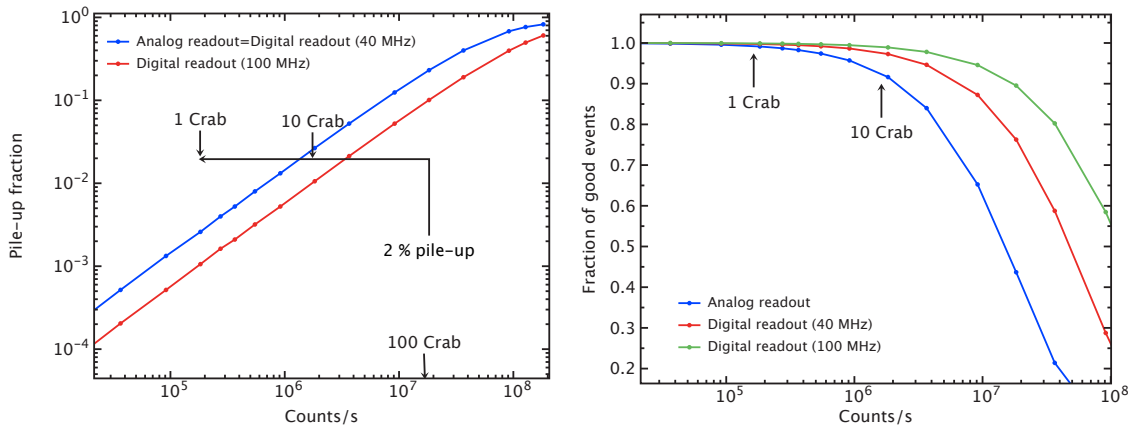

Figure 12: Left) HTRS simulated pile-up performance as a function of the input count rate for both the analog and digital readouts (this assumes $T_2 = 200$ ns for the analog and digital option with an ADC rate of 40 MHz, and $T_2 = 80$ ns for the digital readout with an ADC speed of 100 MHz. Right) HTRS detection efficiency as a function of input count rate for the three solutions, as defined as the fraction of good events for which both the energy and arrival time are measured.

displayed in Fig. 12 for different source brightness. As can be seen, both solutions match the top level HTRS requirement of handling a 1 Crab source with less than 2% pile-up. Clearly the use of high speed ADCs can further improve the count rate performance of the instrument.

4. Data modes and data rates

The HTRS can handle bright sources with fluxes of 1 Crab and more, resulting in event rates of 170000 counts/sec and higher. This corresponds to raw data rates of up to and exceeding 5 Mbit/s if individual events were transmitted. As in the ESA study the telemetry allocated to the HTRS is only 840 kbit/s (for a duration equivalent to the observation length), however, transmitting single

event information would only be possible in the case of observations of the faintest HTRS targets. For the majority of observations, it is therefore necessary to employ data compression strategies that allow to encode all scientifically relevant information within the permitted telemetry envelope.

For a typical astronomical data set, Monte Carlo studies show that the compression ratio for simple event lists (i.e., a stream of time tags and SDD and energy information) is only up to 50%, even when using very efficient (and CPU-intensive) data compression algorithms such as bzip2. The same studies show that significantly higher compression ratios of up to a factor of 5 and more are possible in a so-called "compressed binned data mode". The heritage of this data mode are the "science archive" data modes implemented in the experiment data system (EDS) of the Rossi X-ray Timing Explorer (see Appendix F to the RXTE NRA). In contrast to the RXTE, however, the implementation of the data mode is mainly in software in the DPU and not entirely in dedicated hardware.

In the first step of forming data packets for the compressed binned data mode, event data from individual SDDs are energy corrected onto a set of pulse invariant energy channels. In a second step spectra are accumulated from all events measured within a given time. Depending on the scientifically required time resolution, such spectra can be measured with sampling frequencies of up to 4096 Hz (definable by the observer). With 256 energy channels per spectrum, the energy response of the SDDs can be oversampled sufficiently enough for most scientific questions, however, it is foreseen that the exact energy binning can be influenced by the observer. In a third step, these spectra are then compressed using a compression algorithm such as gzip or bzip2. Our studies show that modern space-qualified processors are sufficiently fast to allow this step to be performed in software, i.e., no hardware compression is necessary. Since the available compression algorithms are very efficient in removing unused zeros, this approach also allows us to use 16 bit registers during the spectral accumulation, thereby avoiding integer overflows.

Monte Carlo studies show that for the majority of HTRS targets, this approach allows to stay within the allocated telemetry limits. Because the compression ratio depends on the source behavior, however, observations of few bright sources could still generate data rates greater than the telemetry rate. In this particular case it is foreseen to store the remaining data on-board in an internal mass memory and download it during observations of sources generating a compressed data rate lower than 840 kbit/s. In order to size this internal mass memory, Monte Carlo simulations based on realistic one year observing plans were performed, assuming that 4.8 Msec are dedicated to the HTRS. For each observation, spectral and temporal resolution are set according to realistic science goals. These realistic simulations show that even in worst case, 64 Gbits of mass memory are sufficient to ensure the storage and eventual download of all HTRS science data.

In addition to the science data described above, for all observations the HTRS also provides highly compressed data in a standardized format that is independent of the settings of the binned data mode and ensures that directly comparable data are taken for all sources with the HTRS. These standardized modes are still under discussion, with the baseline consisting i) a binned mode with 1ms time resolution and 4 wide energy channels covering the full HTRS band, ii) a binned mode with full energy resolution (256 channels) and a time resolution of 1s, and iii) event data taken at full energy and time resolution for 1s every 512 s. In total, the telemetry requirement for these standard data is 0.1 Mbit/s. These standard data could be telemetered to Earth with higher priority than the more voluminous compressed binned data mode packets, to allow observers quick

feedback on the behavior of the target.

5. Conclusions

As designed, the HTRS relies on existing technologies, which all have a high technology readiness level, building up from significant space heritage. Its electrical, mechanical and thermal designs have reached a high level of maturity, along the assessment study phase concluded in mid-2010. Performance simulations have provided support for design evolutions and trade-off analysis. The current HTRS design meets the top level requirement defined for IXO ($>$ 90% throughput at 1 Crab) with very safe margins. Funding is in place to terminate the main HTRS related hardware activities (ASIC, digital shaper, ...). The recent abandon of IXO implies a reconfiguration of the payload for the European-led mission, and a drop of the HTRS as a stand-alone instrument. It is already certain that the work accomplished for the HTRS will not be wasted, and will be useful for implementing a high count rate capability for the new mission.

Acknowledgements

It is a pleasure to thank all the members of the ESA and NASA of the project teams, led by Nicola Rando (ESA) and Jean Grady (NASA). Special thanks to Didier Martin, IXO study payload manager and his team, for helpful comments along the instrument definition review and mid-term review. The HTRS effective area curves have been computed by Tim Oosterbroek (ESA). The research presented in this paper was funded in part by Bundesministerium fuer Wirtschaft und Technologie under Deutsches Zentrum fuer Luft- und Raumfahrt grants 50 QR 0901-03.

We are grateful to their continuous support and interests to the HTRS on IXO: D. Altamirano, A. Baykal, S. Bhattacharyya, T. Belloni, E. Cackett, P. Callanan, D. Chakrabarty, M. Diaz-Trigo, C. Done, K. Ebisawa, S. Farrell, M. Gilfanov, E. Gogus, E. Gourgoulhon, J. Homan, W. Hermsen, P. Jonker, E. Kalemnci, Ph. Kaaret, E. Kendziorra, M. van Kerkwijk, M. van der Klis, W. Kluzniak, C. Kouvelioutou, D. Lai, J.P. Lasota, T. Maccaronne, K. Makishima, C. Miller, J.F. Olive, F. Paerels, I. Papadakis, J. Paredes, J. Poutanen, D. Psaltis, N. Réa, R. Remillard, M. Revnivtsev, J. Rodriguez, R. Rothschild, L. Stella, M. Tagger, J. Tomsick, H. Tsunemi, Y. Uchiyama, A. Watts, R. Wijnands, J. in't Zan't, A. Zdziarski.

References

[1] X. Barcons, D. Barret, M. Bautz, J. Bookbinder, J. Bregman, T. Dotani, K. Flanagan, R. Fraga-Encinas, J. Grady, H. Kunieda, D. H. Lumb, K. Mitsuda, K. Nandra, T. Ohashi, L. Piro, N. Rando, L. Strüder, T. Takahashi, T. G. Tsuru, and N. E. White, "International X-ray Observatory (IXO) Assessment Study Report for the ESA Cosmic Vision 2015-2025," *ArXiv e-prints* , Feb. 2011.

[2] D. Barret, T. Belloni, S. Bhattacharyya, M. Gilfanov, E. Gogus, J. Homan, M. Méndez, J. M. Miller, M. C. Miller, S. Mereghetti, S. Paltani, J. Poutanen, J. Wilms, and A. A. Zdziarski, "Science with the XEUS high time resolution spectrometer," in *Society of Photo-Optical Instrumentation Engineers (SPIE) Conference Series, Society of Photo-Optical Instrumentation Engineers (SPIE) Conference Series* **7011**, Aug. 2008.

[3] P. Lechner, S. Eckbauer, R. Hartmann, S. Krisch, D. Hauff, R. Richter, H. Soltau, L. Strüder, C. Fiorini, E. Gatti, A. Longoni, and M. Sampietro, "Silicon drift detectors for high resolution room temperature X-ray spectroscopy," *Nuclear Instruments and Methods in Physics Research A* **377**, pp. 346–351, Feb. 1996.

[4] A. Niculae, P. Lechner, H. Soltau, G. Lutz, L. Strüder, C. Fiorini, and A. Longoni, "Optimized readout methods of silicon drift detectors for high-resolution X-ray spectroscopy," *Nuclear Instruments and Methods in Physics Research A* **568**, pp. 336–342, Nov. 2006.

[5] P. Lechner, W. Buttler, C. Fiorini, R. Hartmann, J. Kemmer, N. Krause, P. Leutenegger, A. Longoni, H. Soltau, D. Stoetter, R. Stoetter, L. Strueder, and U. Weber, "Multichannel silicon drift detectors for x-ray spectroscopy," in *Society of Photo-Optical Instrumentation Engineers (SPIE) Conference Series*, J. E. Truemper & B. Aschenbach, ed., *Society of Photo-Optical Instrumentation Engineers (SPIE) Conference Series* **4012**, pp. 592–599, July 2000.

[6] P. Lechner, C. Amoros, D. Barret, P. Bodin, M. Boutelier, R. Eckhardt, C. Fiorini, E. Kendziorra, K. Lacombe, A. Niculae, B. Pouilloux, R. Pons, D. Rambaud, L. Ravera, C. Schmid, H. Soltau, L. Strüder, C. Tenzer, and J. Wilms, "The silicon drift detector for the IXO high-time resolution spectrometer," in *Society of Photo-Optical Instrumentation Engineers (SPIE) Conference Series*, *Presented at the Society of Photo-Optical Instrumentation Engineers (SPIE) Conference* **7742**, July 2010.

[7] G. Segneri, C. Brown, J.-D. Carpenter, B. Kuhnle, T. Lauf, P. Lechner, G. Lutz, S. Rummel, L. Struder, J. Treis, and C. Whitford, "Measurement of the current related damage rate at -50 c and consequences on macropixel detector operation in space experiments," *IEEE TNS* **56**(6), p. 3734 3742, 2009.

[8] C. Schmid, M. Martin, J. Wilms, I. Kreykenbohm, M. Mühlegger, H. Brunner, M. Fürmetz, P. Predehl, E. Kendziorra, and D. Barret, "Simulations of X-Ray Telescopes for eROSITA and IXO," in *American Institute of Physics Conference Series*, A. Comastri, L. Angelini, & M. Cappi, ed., *American Institute of Physics Conference Series* **1248**, pp. 591–592, July 2010.

[9] R. Klein and S. Roberts, "A time-varying poisson arrival process generator," *Simulations* **43**(4), pp. 193–195, 1984.

[10] J. Timmer and M. Koenig, "On generating power law noise.," *A&A* **300**, pp. 707–+, Aug. 1995.